How to Analyze the Neurodynamic Characteristics of Pulse-Coupled Neural Networks? A Theoretical Analysis and Case Study of Intersecting Cortical Model

Xin Jin, *Member, IEEE*, Dongming Zhou, Qian Jiang, Xing Chu, *Member, IEEE*, Shaowen Yao, *Member, IEEE*, Keqin Li, *Fellow, IEEE*, and Wei Zhou, *Member, IEEE*

Abstract—The intersecting cortical model (ICM), initially designed for image processing, is a special case of the biologically inspired pulse-coupled neural-network (PCNN) models. Although the ICM has been widely used, few studies concern the internal activities and firing conditions of the neuron, which may lead to an invalid model in the application. Furthermore, the lack of theoretical analysis has led to inappropriate parameter settings and consequent limitations on ICM applications. To address this deficiency, we first study the continuous firing condition of ICM neurons to determine the restrictions that exist between network parameters and the input signal. Second, we investigate the neuron pulse period to understand the neural firing mechanism. Third, we derive the relationship between the continuous firing condition and the neural pulse period, and the relationship can prove the validity of the continuous firing condition and the neural pulse period as well. A solid understanding of the neural firing mechanism is helpful in setting appropriate parameters and in providing a theoretical basis for widespread applications to use the ICM model effectively. Extensive experiments of numerical tests with a common image reveal the rationality of our theoretical results.

Index Terms—Feature extraction, neural networks, image processing, intersecting cortical model (ICM), neurodynamic analysis, pulse-coupled neural network (PCNN).

Xin Jin, Qian Jiang, Xing Chu, Shaowen Yao, and Wei Zhou are with the School of Software, Yunnan University, Kunming 650091, China (e-mail: xinxin_jin@163.com; jiangqian_1221@163.com; xingchu87@gmail.com; yaosw@ynu.edu.cn; zwei@ynu.edu.cn).

Dongming Zhou is with the School of Information, Yunnan University, Kunming 650091, China (e-mail: zhoudm@ynu.edu.cn).

Keqin Li is with the Department of Computer Science, State University of New York, New Paltz, NY 12561 USA (e-mail: lik@newpaltz.edu).

I. INTRODUCTION

A. Motivation

NEURAL networks are widely used in many fields and have achieved excellent results [1]–[7]. The classical pulse-coupled neural network (PCNN), which is a single-layer, locally connected artificial neural network, was first proposed by Eckhorn [1], [8], [9]. As a multiparameter model, the PCNN is described by five coupled equations, and inappropriate parameter values negatively affect its performance in many applications [10]. Specifically, the PCNN requires at least seven parameters to be set and adjusted manually [11]. This time-consuming process is PCNN's greatest weakness and the source of consistency problems in its applications [12].

The PCNN simulates the information processing mechanisms of some small animals [13], such as feline visual cortex neurons, to simplify the network's computations [14]. However, the computations of the PCNN remain complex and expensive [8]. Therefore, Kinser and Ekblad introduced the PCNN-derived intersecting cortical model (ICM) for image processing in order to simplify the classical versions of the PCNN [15], [16]. Compared with the PCNN, the ICM has a simpler mathematical core and fewer parameters, making the ICM more suitable for image processing in many cases [17]. Although the ICM preserves the basic structure and function of the PCNN model [17], it has a few advantages compared to the PCNN: 1) it has only three parameters, which simplifies setup [18] and 2) it is faster due to its simpler computational model [19]. As a result, the ICM has been widely used since its introduction.

The theoretical foundations of the ICM are given in [15] and [16]. In an ICM network, each neuron represents an individual pixel in the source image. Like the PCNN, the most important features of the ICM are its neural potential accumulation, dynamic threshold, and local communication [20].

Similar to the PCNN, a group of similar neurons in an ICM network can output synchronous pulses under the effect of mutual-coupled pulses [21], [22], in which the synchronous pulses of neurons are treated as 0 or 1 [23]. After several iterations, the output of the ICM is a series of binary images representing the features of the input image (signal) [12]. In

particular, the model parameters, input image pixel value, and surrounding neuron states determine the output of an ICM neuron [24]. Of these three, the parameters are the only controls fully definable by the user. The input image pixel value is independent. The influence of the surrounding neuron states is determined by the synaptic window, which is set in the traditional manner. Thus, the parameter of the ICM is the only settable property, and this property has a significant effect on the performance.

As shown by the application of the PCNN for image segmentation [25] and image fusion [26], the neurodynamic analysis of an ICM can benefit performancewise from careful parameter tuning, especially since the parameters related to the invalid condition and pulse period of the ICM neurons are two important issues. By analyzing the invalid condition of a neuron, the relationship between the parameters and the input signal are useful for improving ICM performance. Furthermore, the pulse period is useful for understanding the firing mechanism of ICM neurons and adjusting the parameters of each neuron. However, the complexity of the continuous firing condition and neural pulse period analysis means that comparatively little research into their definitions has been done. Consequently, ICM networks have had limited application in many fields.

B. Our Contributions

The ICM is one of the most widely used neural networks for image processing. However, current work emphasizes ICM applications rather than neurodynamic analyses, especially relating to the invalid condition and firing pulse period in ICM neurons. For this reason, we investigate the invalid condition and pulse period of ICM neurons based on an analysis of a neuron's internal state, which reveals the firing mechanism of an ICM network to provide a transferable theory. As far as we know, our research is the first neurodynamic analysis of the ICM. Our contributions are as follows.

First, we deduce the conditions for the continuous firing of an ICM neuron, known as an invalid condition, according to the neuron's internal activity. This allows us to assess the relationship between the parameters and the input signal, which indicates whether an ICM network can work well in a specific application. This result can be used for setting parameters, which can make the ICM model easier to use.

Second, we evaluate the pulse period of an ICM neuron based on its firing condition to understand the firing mechanism of a neuron. This understanding guides parameter selection and optimization. Furthermore, the pulse period of an ICM neuron is ultimately useful in reducing the complexity of parameter selection in view of the invalid condition. This method verifies a theory to create a PCNN network that functions well.

Finally, we deduce the relationship between the invalid condition and firing period of each neuron to confirm the rationality of each one, which demonstrates the validity of our conclusions. We also provide experimental results that validate our mathematical derivations and conclusions. This idea provides an available way to study other PCNN models.

The remainder of this article is organized as follows. In Section II, we describe related works, and in Section III, we introduce the ICM neural network. In Section IV, we analyze the continuous firing condition of an ICM neuron, including nonlinking and linking ICM networks. In Section V, we investigate the firing period of an ICM neuron, and in Section VI, we derive the relationship between the continuous firing condition and the firing period of an ICM neuron. In Section VII, we present our experiments and results. The conclusions are provided in Section VIII.

II. RELATED WORKS

Ekblad and Kinser first proposed the ICM neural network in 2004 for image change detection, which proved useful in applications including aircraft, cars, and nuclear explosion tests [15], [16], [27]. The ICM's advantages have led to its wide use in image processing for tasks, such as feature extraction, image segmentation, image denoising, and image fusion.

The coupled pulse characteristic of the ICM network makes it efficient for image feature extraction. Xu *et al.* [28] proposed an iris feature-extraction method based on the ICM that was used to extract the features of the enhanced iris image. Others proposed a facial feature-extraction method using a segmented face as the input of an ICM network to obtain the binary images of the features of the source face image [29]. The ICM has also been applied to geometry-invariant texture retrieval in combination a with support vector machine [30]. These works have shown that ICM-extracted pulse features are more effective than the classic Gabor features in runtime and retrieval accuracy. Furthermore, ICMs have been used for image matching [31], plant recognition [32], unstructured lane detection [33], and human face recognition [34].

ICM networks have also been used for image segmentation. ICM's coupled pulse and wave propagation behavior make it possible to extract regional features of an image that are useful for image segmentation. Automatic segmentation of the nuclei in reflectance confocal microscopy images has been proposed; this applies an ICM and an artificial neural-network classifier to an image model of nuclei with varying contrast [24]. Gao *et al.* [35] utilized a clustering algorithm to separate the image pixels; thus, a dynamic linear threshold attenuation can be used as the linking synaptic matrix of ICM for image segmentation. In the study of Wang *et al.* [20], a saliency guided ICM was used for object segmentation based on an adaptive and simple threshold. Zhen [36] combined the ramp width reduction with ICM to avoid the geometric distortion problem. Tan and Ashidi [37] used ICM to segment the sperm head region in an image with the parameters selected by particle swarm optimization using feature mutual information as the objective function. Similarly, Lakshmi and Ravi [18] employed a cuckoo search optimization algorithm to find the parameters of ICM, which can improve the performance of the segmentation algorithm. In image segmentation, the parameter selection of ICM is a challenging problem, and the optimization algorithms are usually used to find the optimized parameters, which need a large amount of computing resources.

From its introduction in 1989, image fusion has received significant attention. The regional and detailed features are important to image fusion, and the synchronous pulse and wave propagation of ICMs represent these features well. The physiological motivation is shown by Broussard et al. [26]. ICMs were first used for image fusion in combination a with wavelet transform [38]. Later, they were combined with a discrete Ripplet transform for multimodal medical image fusion [39]. Kong [40] proposed a transform-domain-based image fusion method by combining a modified ICM with a nonsubsampled shearlet transform. In 2016, an ICM was combined with a PCNN and NSST for remote-sensing image fusion [41]. Wang et al. [42] proposed an image-fusion method based on an ICM combined with the composite image-clarity criterion and incorporated an adaptive iteration number-setting method dependent on the size of the source image instead of using a constant. Yang first proposed an image fusion method based on NSST and ICM [43]; and then Yang and Wang made some small changes for ICM to improve image fusion performance [44]. A modified ICM was also proposed by Li et al. to fuse the low- and high-frequency coefficients of source images in the surfacelet domain [45]. Xin et al. [12] employed ICM to extract the features of medical images in the NSST domain. In image fusion, the out pulses of ICM are usually used to present the detail distribution of different source images, and the ICM is also combined with multiscale analysis methods.

The synchronous pulse and dynamic threshold of an ICM are suitable for image denoising. Yuan et al. [46] used an ICM to identify the noisy pixels that will be removed in each channel of color images. Similarly, another ICM noise-removal method for color images was proposed that incorporated an automatic window-selecting method [47]. Zhang et al. [48] combined an ICM and an improved extremum-and-median filter for image denoising. In the research of Nisha and Mohideen [49], four different variants of PCNN including ICM were, respectively, combined with four popular filters to remove medical image noise. In general, ICM is often combined with filter techniques for image denoising.

In addition to the preceding, ICMs have also been used for other image processing tasks, such as image enhancement [50], object recognition [51], high-dynamic-range image processing [52], realistic image rendition [53], target tracking [54], and edge detection [55].

III. MATHEMATICAL FORMULAS OF ICM

The ICM is a biologically inspired model based on the PCNN technique that is designed to enhance image features without sharp edges or straight lines [15]. It can be regarded as a minimalist version of the PCNN. Fig. 1 is a schematic of a neuron in an ICM network when it is applied to image and 1-D information processing.

During the ICM's iterative process, (1) is the feedback coupled input that receives three inputs: 1) the previous state of the feedback coupled input, as $F_{ij}(n-1)$; 2) the external input, as S_{ij}; and 3) the coupled input generated by surrounding neurons, as $Y_{kl}(n-1)$. The firing threshold of a neuron changes
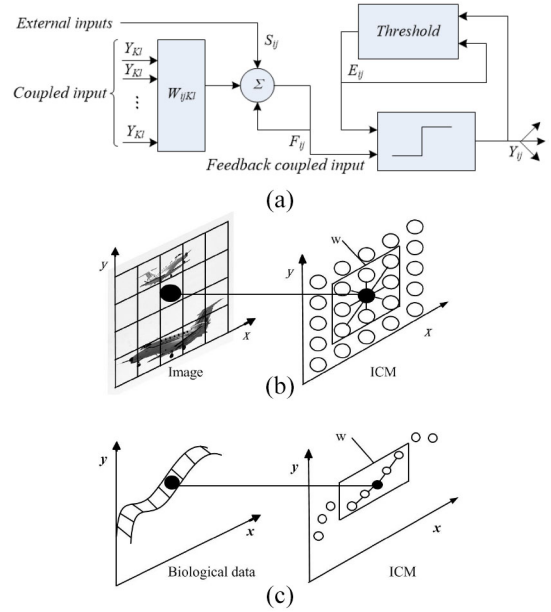

Fig. 1. Diagram of an ICM for signal processing [10], [56]. (a) ICM neuron. (b) ICM in 2-D signal processing. (c) ICM in 1-D signal processing.

dynamically according to its previous state and previous output generated by the neuron, as shown in (2). The nonlinear pulse generator generates pulses according to the feedback coupled input and dynamic threshold, as shown in (3). When the internal activity is larger than the dynamic threshold, the neuron activates and outputs a pulse (called firing or ignition) [46]. In the ICM, the variables of a neuron satisfy

$$F_{ij}(n) = fF_{ij}(n-1) + \sum_{kl} W_{ijkl}Y_{kl}(n-1) + S_{ij} \quad (1)$$

$$E_{ij}(n) = gE_{ij}(n-1) + hY_{ij}(n-1) \quad (2)$$

$$Y_{ij}(n) = \begin{cases} 1, & F_{ij}(n) > E_{ij}(n) \\ 0, & \text{otherwise} \end{cases} \quad (3)$$

where subscript (i, j) is a neuron's position with (k, l) representing the positions of its surrounding neurons, n is the current iteration number less than or equal to the maximum iteration number N, F_{ij} is the feedback coupled input, E_{ij} is the dynamic threshold, Y_{ij} is the output firing status of neuron (i, j) regarded as the nonlinear pulse generator, S_{ij} is the external input image (signal) and it is constant throughout the N iteration, W_{ijkl} is the connection function representing communication between the central neuron and its surrounding neurons, and the values are usually set as positive numbers manually, f and g denote time decay constants, and they are both smaller than 1 but larger than 0, as $0 < g < 1$ and $0 < f < 1$, and h is a positive amplification coefficient. For the sake of consistency in this article, we take the parameter values $f = 0.85$, $g = 0.5$, and $h = 15$ as an example.

Each neuron represents a unique pixel of the input image, and its status is affected by the image pixel value and the status of surrounding neurons [24]. The capture characteristics of the neuron lead to the surrounding similar neurons' capturing its output, automatically coupling the neurons and transmitting the ignition information. In each iteration, a binary image is

obtainable by recording the fire or no-fire status of neurons in the network, and the image can be regarded as the features of the input image because the pixel position of source image corresponds to the position of a firing statistics graph (FSG) [10]. After the addition of all the binary images, the FSG is found using the equation

$$\text{FSG}(ij) = \sum_{n=1}^{N} Y_{ij}(n) \tag{4}$$

where N denotes the maximum iteration number and Y_{ij} is the output pulse of neuron (i, j).

IV. ANALYSIS OF CONTINUOUS FIRING CONDITION OF ICM NEURON

In some cases, ICM neurons may continuously fire, that is, producing an output pulse at each iteration. If all ICM neurons fire continuously, the entire network is invalid as the outputs do not represent the features of the input signal. The pulse transmission and coupling mechanism leading to this situation has been proven in many applications [59]. In this section, we analyze the invalid state to determine parameters that avoid it.

A. Analysis of Continuous Firing Condition of Nonlinking ICM Neuron

In this section, we examine the continuous firing condition of nonlinking neurons to determine the applicable restrictions between the parameters and input signal, because each neuron will operate without the influence of its surrounding neurons. This makes the mechanism analysis simple and can help us obtain basic theoretical results. Besides, the operating mechanism of uncoupled neurons is also important to the firing behavior of the ICM. When a nonlinking ICM is applied to image processing, the input is generally simplified as itself and the external input signal S, describing the neuron according to

$$F(n) = fF(n-1) + S \tag{5}$$

$$E(n) = gE(n-1) + hY(n-1) \tag{6}$$

$$Y(n) = \begin{cases} 1, & F(n) > E(n) \\ 0, & \text{otherwise.} \end{cases} \tag{7}$$

Theorem 1: For a nonlinking ICM, if $f > 0$, the feedback input can be represented as

$$F(n) = S\frac{1 - f^n}{1 - f}.$$

Proof: Suppose F represents the feedback input, with initial state $F(0) = 0$ and S represents the external input signal. Consequently, the feedback input increases according to (5), with $F(1)$, $F(2)$, $F(3)$, $\cdots$, and $F(n)$ described as

$$F(0) = 0$$
$$F(1) = fF(0) + S = S$$
$$F(2) = fF(1) + S = fS + S$$
$$F(3) = fF(2) + S = f(fS + S) + S = f^2S + fS + S$$
$$\vdots$$
$$F(n) = S\frac{1 - f^n}{1 - f}. \tag{8}$$

Equation (8) shows that the feedback input F of a nonlinking ICM neuron will increase with increasing iterations.

The proof is completed. ∎

Theorem 2: For a nonlinking ICM, if $g > 0$ and $h > 0$, the dynamic threshold can be represented as

$$E(n) = h\frac{1 - g^n}{1 - g}.$$

Proof: Suppose E represents the dynamic threshold with initial state $E[0] = 0$, and Y represents the output with initial state $Y[0] = 0$. For a continuously firing neuron, its output maintains the state $Y(n) = 1$ because the firing condition $F(n) > E(n)$ is always satisfied. As a result, the dynamic threshold keeps increasing according to (6), with $E(1)$, $E(2)$, $E(3)$, $\cdots$, and $E(n)$ described as

$$E(0) = 0$$
$$E(1) = gE(0) + h = h$$
$$E(2) = gE(1) + h = gh + h$$
$$E(3) = gE(2) + h = g(gh + h) + h = g^2h + gh + h$$
$$\vdots$$
$$E(n) = h\frac{1 - g^n}{1 - g}. \tag{9}$$

Equation (9) shows that the dynamic threshold E of nonlinking ICM neurons will increase as the iterations increase.

The proof is completed. ∎

Since nonlinking ICM neurons continuously fire, the firing condition $F(n) > E(n)$ is always satisfied. According to (8) and (9), the continuous firing condition can be described by

$$F(n) = S\frac{1 - f^n}{1 - f} > E(n) = h\frac{1 - g^n}{1 - g}. \tag{10}$$

Theorem 3: For a continuously firing nonlinking ICM neuron, the continuous firing condition in (10) can be represented as

$$S > h\frac{(1 - f)}{(1 - g)}, n \to \infty.$$

Proof: Equation (10) can be further represented as

$$S\frac{(1 - f^n)}{(1 - f)} > h\frac{(1 - g^n)}{(1 - g)}. \tag{11}$$

Rewriting the equation leads to the continuous firing condition expressed as

$$S > h\frac{(1 - g^n)(1 - f)}{(1 - g)(1 - f^n)}. \tag{12}$$

When n goes to infinity, (12) can be represented as

$$S > h\frac{(1 - f)}{(1 - g)}. \tag{13}$$

Equation (13) is the continuous firing condition of a nonlinking ICM neuron.

The proof is completed. ∎

To verify the rationality of the analysis in this section, we employ a set of common parameters and signals as examples.
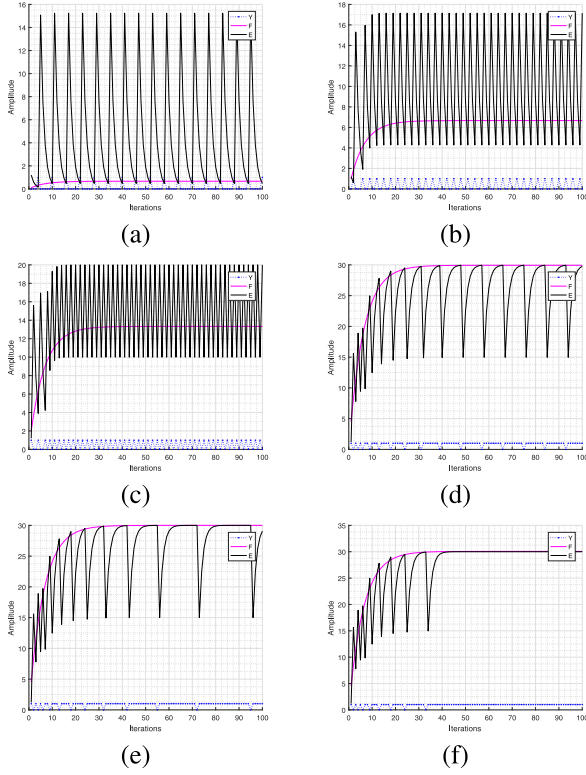
Fig. 2. Neuron activity status for different inputs: (a) In=0.1; (b) In=1; (c) In=2; (d) In=4.49; (e) In=4.5; and (f) In=4.51.

Example 1: For parameter values $f = 0.85$, $g = 0.5$, and $h = 15$, the continuous firing condition can be calculated according to (13)

$$S > h\frac{(1-f)}{(1-g)} = 4.5.$$

Fig. 2 shows the active states of an ICM neuron for different input signals. The blue line shows Y, with the peaks representing the output pulse. The symbol *In* represents a variable element of the input signal. After many iterations, we obtain two results.

1) When $In = 0.1$, $In = 1$, $In = 2$, and $In = 4.49$, the nonlinking ICM neuron functions properly and fires periodically.
2) When $In = 4.51$, after several changing periodic ignitions, the nonlinking ICM neuron does not function properly and fires continuously.

Per the mathematical derivation (13) in this section, when the input signal is below the continuous firing condition (e.g., $S > 4.5$), the nonlinking neuron can function properly, as shown in Fig. 2(a)–(d). However, the performance may be very poor when the input signal approaches the continuous firing condition as shown in Fig. 2(e). If the continuous firing condition is not satisfied, the nonlinking ICM neuron cannot function properly, as shown in Fig. 2(f). The experiments prove the validity of the continuous firing condition as discussed in this section.

In this section, the external input signal must be less than the calculated S value from (13), which is the continuous firing condition that ensures that the neuron maintains its normal working status. Fig. 2(a)–(d) shows that the neuron outputs a cycle pulse when the external input signal is less than S. Fig. 2(f) shows that when the external input signal is larger than S, the neuron will remains in the continuous firing condition after several normal cycle pulses.

B. Analysis of Continuous Firing Condition of Linking ICM Neuron

We now analyze the continuous firing condition of a linking ICM neuron to estimate the restrictions between the parameters and input signal. We assume that a linking ICM neuron satisfies (1)–(3).

Theorem 4: For a linking ICM neuron, if $f > 0$, the dynamic threshold can be represented as

$$F(n) = S\frac{1-f^n}{1-f} + \sum_{i=0}^{n-1} X(i)\frac{1-f^{n-i-1}}{1-f}.$$

Proof: Let $\sum_{kl} W_{ijkl}Y(n-1)$ be represented by $X(i)$, and the initial state of the linking ICM neuron is also $F[0] = 0$, $Y(0) = 0$, and $X(0) = 0$. Thus, the feedback input keeps increasing according to

$$F(n) = fF(n-1) + S + X(i). \tag{14}$$

Then, we can describe $F(1)$, $F(2)$, $F(3)$, $\cdots$, and $F(n)$, as follows:

$$F(0) = 0$$
$$F(1) = S + X(0) = S$$
$$F(2) = fF(1) + S + X(1)$$
$$F(3) = fF(2) + S + X(2) = f^2 S + fS + fX(1) + S + X(2)$$
$$\vdots$$
$$F(n) = S\frac{1-f^n}{1-f} + \sum_{i=0}^{n-1} X(i)\frac{1-f^{n-i-1}}{1-f}. \tag{15}$$

Equation (15) shows that the dynamic threshold F of a linking ICM neuron increases with the number of iterations. The proof is completed. ∎

The initial state of a linking neuron also has $E[0] = 0$ and $Y[0] = 0$. Since the neuron fires continuously, the output is always $Y(n) = 1$, with the dynamic threshold $E(n)$ as described by (9). The firing condition $F(n) > E(n)$ described by (16) must be always satisfied as well, taking into account the contribution of surrounding neurons as $X(i) \in [0, \text{sum}(W)]$

$$F(n) = S\frac{1-f^n}{1-f} + \sum_{i=0}^{n-1} X(i)\frac{1-f^{n-i-1}}{1-f} > E(n) = h\frac{1-g^n}{1-g}. \tag{16}$$

Theorem 5: If $f > 0$, $g > 0$, and $h > 0$, a linking ICM neuron fires continuously in accordance with the following representation:

$$S > \left(h\frac{1-g^n}{1-g} - \sum_{i=0}^{n-1} X(i)\frac{1-f^{n-i-1}}{1-f}\right)\frac{1-f}{1-f^n}.$$

Proof: Equation (16) can be rewritten as

$$S\frac{1-f^n}{1-f} + \sum_{i=0}^{n-1} X(i)\frac{1-f^{n-i-1}}{1-f} > h\frac{1-g^n}{1-g}. \quad (17)$$

From this, we obtain the linking ICM neuron's continuous firing condition as

$$S\frac{1-f^n}{1-f} > h\frac{1-g^n}{1-g} - \sum_{i=0}^{n-1} X(i)\frac{1-f^{n-i-1}}{1-f}$$

$$S > \left(h\frac{1-g^n}{1-g} - \sum_{i=0}^{n-1} X(i)\frac{1-f^{n-i-1}}{1-f}\right)\frac{1-f}{1-f^n}. \quad (18)$$

Equation (18) is the continuous firing condition of a linking ICM neuron.

The proof is completed. ∎

Since this section considers an ICM neuron in an invalid status, we assume that the central neuron and its surrounding neurons are all firing continuously, such that $Y_{ijkl}(n-1) \equiv 1$, and we can obtain $X(i) = \text{sum}(W)$, in which $\text{sum}(W)$ means the summation of its elements. All surrounding neurons remain continuously firing, influencing the central neuron to fire continuously. As a result, the continuously firing condition of a linking ICM neuron is described in

$$S > \left(h\frac{1-g^n}{1-g} - \text{sum}(W)\frac{1-f^{n-1}}{1-f}\right)\frac{1-f}{1-f^n}$$

$$> h\frac{1-g^n}{1-g}\frac{1-f}{1-f^n} - \text{sum}(W)$$

$$S > h\frac{1-g^n}{1-g}\frac{1-f}{1-f^n} - \text{sum}(W). \quad (19)$$

When n tends to infinity, we obtain (20)

$$S > h\frac{1-f}{1-g} - \text{sum}(W). \quad (20)$$

To verify the correctness of the mathematical derivation in this section, we input different 1-D input signals to linking ICM neurons while surrounding neurons simultaneously input different signals in an experiment.

Example 2: We set the following parameters in our linked ICM neuron: $W = [1/4, 1/3, 0, 1/3, 1/4]$, $f = 0.85$, $g = 0.5$, and $h = 15$. Since the firing state of the surrounding neurons is very difficult to deduce by mathematical analysis, (19) and (20) can be used to obtain a rough analysis of the continuous firing of a linking ICM neuron.

In a linking ICM neuron, the continuous firing condition can be calculated as

$$S > h\frac{1-f}{1-g} - \text{sum}(W) = 4.5 - \frac{7}{6} \approx 3.3333. \quad (21)$$

Figs. 3 and 4 show the results when different surrounding input signals are input into a linking ICM neuron. When the input signal is set as $Ins = [3, 8, In, 7, 9]$, the activity states of the neuron are as shown in Fig. 3. When the input signal is set as $Ins = [0.3, 0.8, In, 0.7, 0.9]$, the activity sates of a linking ICM neuron are as shown in Fig. 4. The former signal values are larger than the normalized signal to ensure that the surround neurons keep firing. The latter signal values are
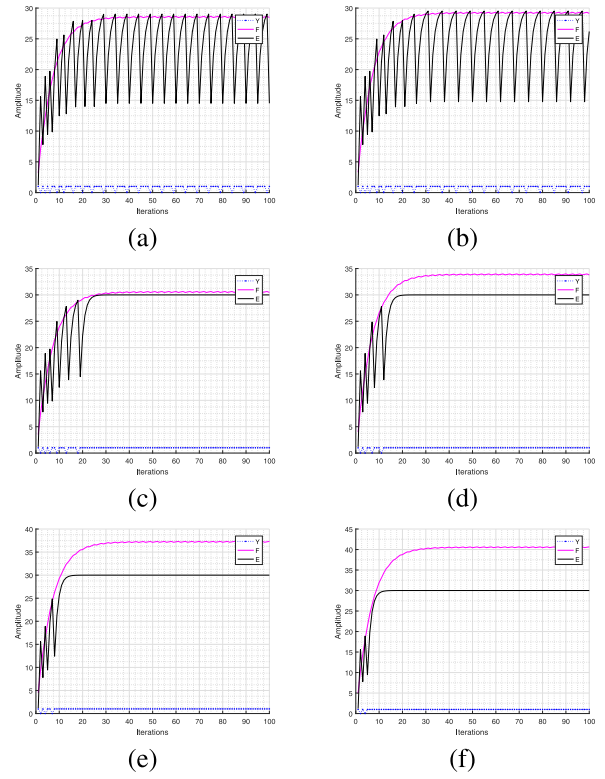

Fig. 3. Neuron activity states of different inputs with surrounding input signals Ins=[3, 8, In, 7, 9]: (a) In=3.2; (b) In=3.3; (c) In=3.5; (d) In=4; (e) In=4.5; and (f) In=5.

smaller than the normalized signal to decrease the impact on the central linking neuron.

Furthermore, when the input signal is below the continuous firing condition of the linking neuron according to (21), such as $In = 3.3$ in Figs. 3 and 4, the linking neuron functions properly. If the input signal is above the condition, the linking neuron does not function properly. Furthermore, as the input signal increases, the neuron continues to fire without interruption.

Specifically, when the input signal is below the continuous firing condition of a linking neuron, as with $S > 3.3333$, the surrounding neurons are more likely to remain continuously firing. The linking neuron functions properly as shown in Fig. 3(a) and (b). When the input signal is greater than the continuous firing condition, the linking neuron will remain in the continuous firing state and no longer function properly after several changing periodic ignitions as shown in Fig. 3(c)–(f).

In Fig. 4, when the input signal is below the continuous firing condition of a linking neuron, as when $S > 3.3333$, the surrounding neurons are more likely to maintain noncontinuous firing. The linking neuron functions properly as shown in Fig. 4(a). When the input signal is larger than the continuous firing condition of a nonlinking neuron and smaller than the continuous firing condition of a linking neuron, such as $4.5 > S > 3.3333$, the linking neuron continues functioning properly, as shown in Fig. 4(c). However, when the input signal approaches or exceeds the continuous firing condition, the neuron no longer functions properly, as shown in Fig. 4(d)–(f).
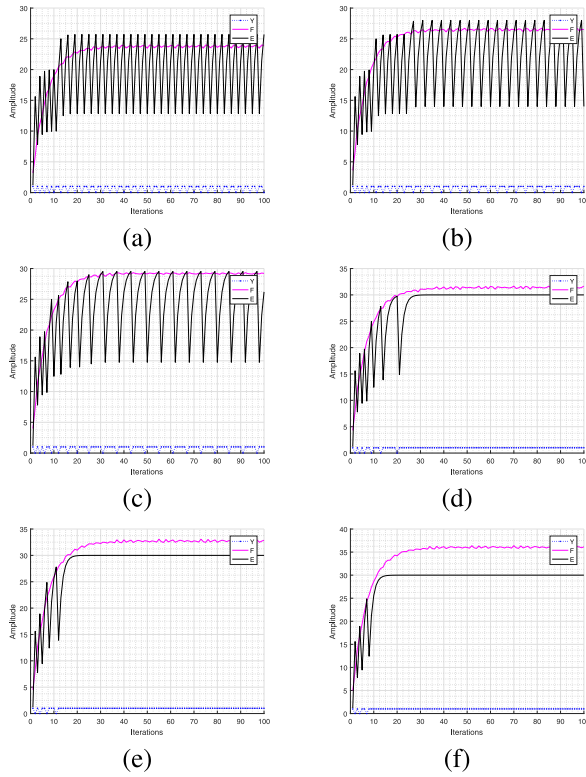
Fig. 4. Neuron activity states of different inputs with surrounding input signal *Ins*=[0.3 0.8 In 0.7 0.9]: (a) *In*=3.2; (b) *In*=3.6; (c) *In*=4; (d) *In*=4.3; (e) *In*=4.5; and (f) *In*=5.

The experimental results in Figs. 3 and 4 show that the external input signal must be below the continuous firing condition of a linking neuron when all surrounding neurons are firing continuously.

V. EVALUATION OF FIRING MECHANISM OF ICM NEURON

An ICM neuron with higher input signal always fires sooner than the one with lower intensity. In this section, we examine the pulse cycle of an ICM neuron to understand the firing mechanism and guide parameter setting to avoid the continuous firing condition. Nie first introduced the definition of the firing period of an ICM neuron [57], [58].

Definition 1: The firing period of an ICM neuron is defined as the iteration interval between two adjacent pulses.

A. Evaluation of Firing Period of Nonlinking ICM Neuron

In this section, we first analyze the firing period of a nonlinking ICM neuron. In a nonlinking neuron, the input signal is normalized into the range of "0–1" with initial states as $F[0] = 0$, $Y[0] = 0$, and $E[0] = 1.2$. It can be inferred that the neuron will not fire during the first iteration, so the corresponding output is $Y[1] = 0$ because the firing condition ($F[1] = S < E[1]$) is not satisfied.

Theorem 6: For a nonlinking ICM neuron, if $f > 0$, $g > 0$, and $h > 0$, the firing period can be described as

$$T(n_m) = n_m - n_{m-1} = \left\lceil \log_g \frac{S}{S_g + h(1-f)} + 1 \right\rceil, m > 1$$

where n represents the nth iteration, and m represents the mth ignition.

Proof: If the neuron does not output the first pulse, (10) increases while (22) decreases at the same time

$$E(n) = gE(n - 1) = g^n E(0). \tag{22}$$

When the firing condition $F(n) > E(n)$ is satisfied, the neuron will output its first pulse, with the firing condition described as

$$F(n) = fF(n - 1) + S = S\frac{1 - f^n}{1 - f} > E(n) = g^n E(0), n > 1. \tag{23}$$

Then, (24) can be obtained according to (23)

$$S\frac{1 - f^n}{1 - f} > g^n E(0)$$
$$\frac{1 - f^n}{g^n} > \frac{(1 - f)E(0)}{S}. \tag{24}$$

From (24), the time of the first pulse of a nonlinking ICM neuron can be obtained.

According to the definition in [57] and [58], the iteration interval between two adjacent pulses is regarded as the firing period of a neuron. We, therefore, assume that a nonlinking neuron outputs the mth pulse at the n_mth iteration and the $(m + 1)$th pulse at the n_{m+1}th iteration. A nonlinking neuron's output pulse at the n_mth iteration means that the dynamic threshold of the next iteration is described by (25) according to (6). If the neuron outputs the next pulse at the n_{m+1}th iteration, (25) satisfies (26) according to (22)

$$E(n_m + 1) = gE(n_m) + Y(n_m)h \tag{25}$$
$$E(n_{m+1}) = g^{(n_{m+1} - n_m - 1)}(gE(n_m) + Y(n_m)h). \tag{26}$$

The feedback input of the n_mth and n_{m+1}th iterations is then described by (27) and (28)

$$F(n_m) = S\frac{1 - f^{n_m}}{1 - f} \tag{27}$$
$$F(n_{m+1}) = S\frac{1 - f^{n_{m+1}}}{1 - f}. \tag{28}$$

When the nonlinking neuron outputs a pulse at the n_{m+1}th iteration, the feedback input should be approximately equal to the dynamic threshold. Furthermore, $F(n_{m+1}) > E(n_{m+1})$ according to (3), which leads to the assumption that the feedback input is approximately larger than the dynamic threshold because their values are very close at this time, as $E(n_{m+1}) \approx F(n_{m+1})$. According to (26), the situation is described by (29) and (30)

$$E(n_{m+1}) = g^{(n_{m+1} - n_m - 1)}(gE(n_m) + h) \approx F(n_{m+1}) \tag{29}$$

$$n_{m+1} - n_m - 1 = \log_g \frac{F(n_{m+1})}{gE(n_m) + h}. \tag{30}$$

Because the iteration must be an integer, we obtain (31)–(33) according to (29) and (30)

$$n_{m+1} - n_m - 1 = \left\lceil \log_g \frac{F(n_{m+1})}{gE(n_m) + h} \right\rceil \tag{31}$$

$$n_{m+1} - n_m = \left\lceil \log_g \frac{F(n_{m+1})}{gE(n_m) + h} \right\rceil + 1 \tag{32}$$

$$n_{m-n_{m-1}} = \left\lceil \log_g \frac{F(n_m)}{gE(n_{m-1}) + h} \right\rceil + 1. \tag{33}$$

Substituting and combining $F(n_m) \approx E(n_m)$, $F(n_{m-1}) \approx E(n_{m-1})$, and (27) and (28) into (33), we obtain the firing period of a nonlinking neuron as follows:

$$T(n_m) = n_m - n_{m-1}$$
$$= \left\lceil \log_g \frac{S(1 - f^{n_m})}{S(1 - f^{n_{m-1}})g + h(1-f)} \right\rceil + 1, m > 1. \tag{34}$$

According to the characteristics of a nonlinking neuron, when the neuron outputs the third pulse or its near future pulses the iteration is quite small; however, the maximum iteration can be considered as infinite in specific applications. Because $0 < f < 1$ and n is quite large, f^n can be regarded as 0. As the result, the firing period of the nonlinking neuron can be described as

$$T(n_m) = n_m - n_{m-1} = \left\lceil \log_g \frac{S}{Sg + h(1-f)} \right\rceil + 1, m > 1. \tag{35}$$

The proof is completed. ∎

Example 3: As an example, we set parameters of a nonlinking neuron as $f = 0.85$, $g = 0.5$, $h = 15$, and $E(0) = 1.2$. Using input signals of $In = 0.001$, $In = 0.1$, $In = 0.5$, and $In = 0.9$, all the inputs satisfy the continuous firing condition of a nonlinking neuron according to (24). The first pulse time can be calculated according to (24), yielding a first pulse period of $T(n_1) = n + 1$. The future pulse periods can be calculated according to (35). Thus, for various input signals, we obtain the following results:

$$In = 0.001, \ T(n_1) = 9, \text{ and } T(n_m) = 13$$
$$In = 0.1, \ T(n_1) = 4, \text{ and } T(n_m) = 6$$
$$In = 0.5, \ T(n_1) = 2, \text{ and } T(n_m) = 4$$
$$In = 0.9, \ T(n_1) = 2, \text{ and } T(n_m) = 3.$$

Fig. 5 shows the resulting pulse periods from the experiments. The blue line denotes Y, the peaks represent the output pulse, and the symbol In represents the input signal.

In Fig. 5(a), for $In = 0.001$, the first pulse period is 9, and then 13 subsequently.

In Fig. 5(b), for $In = 0.1$, the first pulse period is 4, and then 6 subsequently.

In Fig. 5(c), for $In = 0.5$, the first pulse period is 2, and then 4 subsequently.

In Fig. 5(d), for $In = 0.9$, the first pulse period is 2 and the second pulse period is 4, then 3 subsequently.

The mathematical analysis is consistent with the experimental results, which shows that the theoretical analysis is reasonable. It also demonstrates that different input signals In produce different pulse periods.
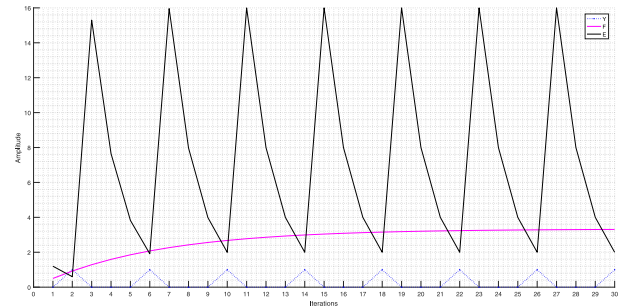
In greater detail, Fig. 5 shows that the results of the mathematical analysis are consistent with the experimental results when the input signal is small. However, when the input signal is large, differences arise between the mathematical analysis
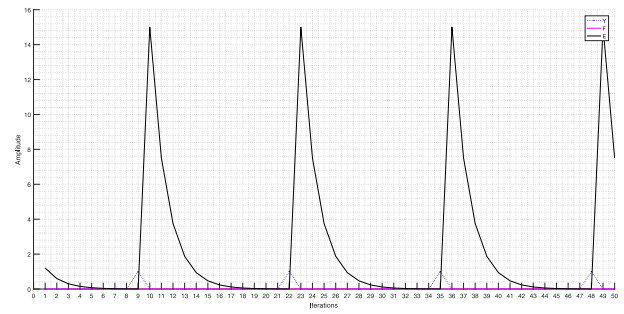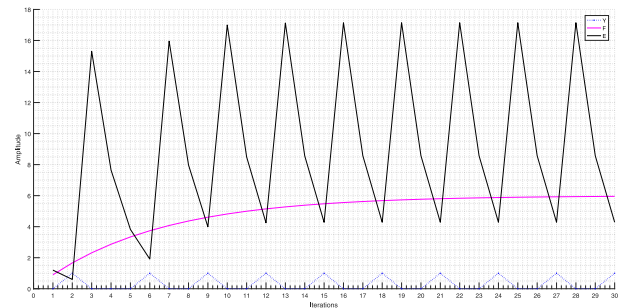

(a)
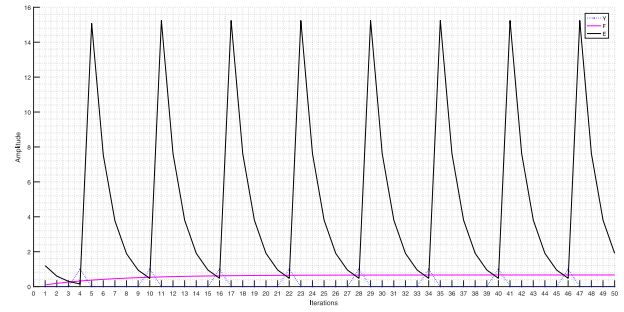
(b)

(c)

(d)

Fig. 5. NonLinking ICM neuron internal state and pulse output time with different inputs: (a) In=0.001; (b) In=0.1; (c) In=0.5; and (d) In=0.9.

and experimental results, although the prediction is largely correct. The cause is that the iteration of the second pulse is small, while f^n does not fully become 0. In addition, a larger input signal In causes the feedback input F to increase quickly, further shortening the pulse cycle. However, Fig. 5 shows that the difference between the mathematical analysis and experimental results is nearly eliminated by the fourth iteration,

with the pulse cycle returning to normal and according with the mathematical analysis. In practical application, the number of iterations is usually large, so the observed pulse cycle will be in accordance with our analytical results.

B. Evaluation of Firing Period of Linking ICM Neuron

In a linking ICM network, similar neurons output synchronous pulses under the influence of mutual coupled pulses. As a result, surrounding neurons exert great influence on the firing behavior of the linking neuron, and the pulse of the linking neuron is output sooner, that is, with a smaller pulse cycle. Because the uncertainty of the input signal will produce uncertain pulses, we cannot obtain a calculable expression for the continuous firing condition of a linking ICM neuron. According to (1)–(3), the feedback input is composed of external incentives and external coupled pulses. The external coupled pulses, in particular, cause the feedback input of a linking neuron to increase faster than that of a nonlinking neuron.

Example 4: In a linking neuron, it is very difficult to predict whether a neuron will output a pulse using mathematical calculation and analysis. Thus, we used experiments to verify the phenomenon of advance firing of linking neurons. We used parameter values $W = [1/4, 1/3, 0, 1/3, 1/4]$, $f = 0.85$, $g = 0.5$, and $h = 15$, and set surrounding input signals to $Ins = [0.3, 0.8, In, 0.7, 0.9]$. We used input signals of $In = 0.001$, $In = 0.1$, $In = 0.5$, and $In = 0.9$.

In Fig. 6, the pulse period of the linking neuron was obtained from the experiments. The blue line indicates output Y, the peaks represent the output pulse, and the symbol In denotes the input signal. In Fig. 6(a), the stable pulse period of a linking neuron occurs sooner than that of a similar nonlinking neuron. The experimental results show that the assumption of the synchronous pulse phenomenon is correct and proves that neurons with higher input signals always fire prior to those of lower intensity. Importantly, Fig. 6 shows that the assumptions of this section are consistent with the experimental results.

VI. Relationship Between Continuous Firing Condition and Firing Period of ICM Neuron

In this section, we deduce the relationship between the continuous firing condition and the firing period of an ICM neuron, which proves the validity of the two results. We also introduce the firing characteristics of nonlinking and linking neurons.
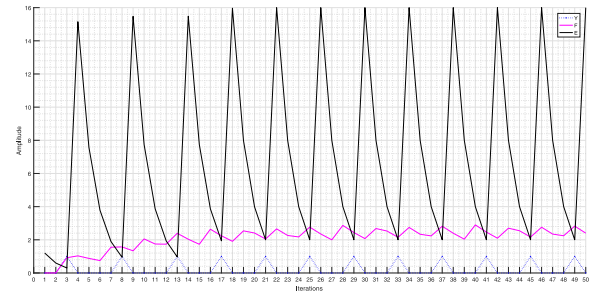
Theorem 7: For a nonlinking neuron with input signal S, $1 > g > 0$ and $h > 0$. The relationship between the pulse period T and g can be represented as follows:
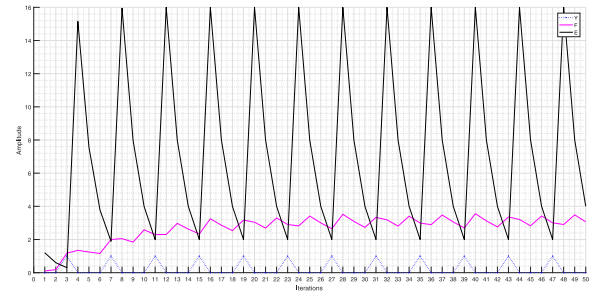
$$g^{T-1}(1 - g) > 1 - g^T.$$

Proof: Using the firing period of a nonlinking neuron from (35), we obtain the following:
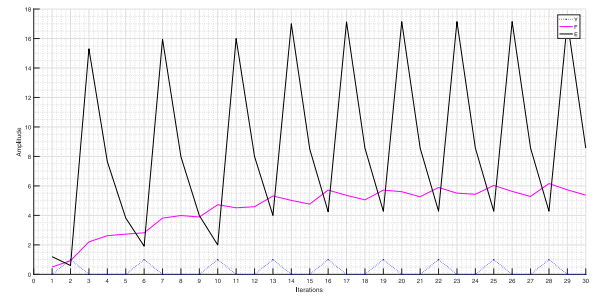
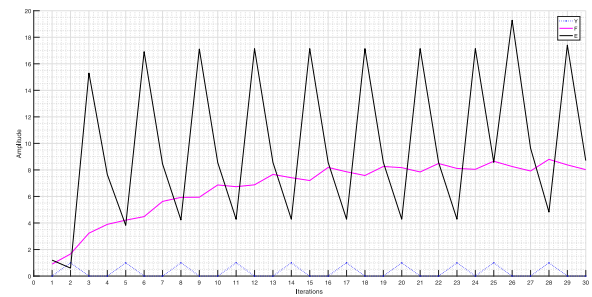$$g^{T-1} > \frac{S}{Sg + h(1 - f)}$$
$$g^{T-1}(Sg + h(1 - f)) = S$$

(a)

(b)

(c)

(d)

Fig. 6. linking ICM neuron internal state and pulse output time for different inputs: (a) In= 0.001; (b)In=0.1; (c) In= 0.5; and(d)In= 0.9.

$$g^{T-1}Sg + g^{T-1}h(1 - f) = S$$
$$g^{T-1}h(1 - f) = S(1 - g^{T-1}g)$$
$$g^{T-1}h(1 - f) = S(1 - g^T) \tag{36}$$

where T represents the firing period of the neuron.

The external input signal S can be described by

$$S = \frac{g^{T-1}h(1 - f)}{(1 - g^T)}. \tag{37}$$

When (13) is satisfied, the neuron is firing continuously, and the ICM neural network is invalid.

Using (13) and (37), we obtain the following:

$$S = \frac{g^{T-1}h(1-f)}{(1-g^T)} > h\frac{1-f}{1-g}$$

$$S = \frac{g^{T-1}}{(1-g^T)} > \frac{1}{1-g}$$

$$g^{T-1}(1-g) > 1 - g^T. \tag{38}$$

The proof is completed. ∎

According to Theorem 7, we find the following inequality, (42), which represents the relationship between T and g

$$g^{T-1} - g^T > 1 - g^T \tag{39}$$

$$g^{T-1} > 1$$

$$T - 1 < 0$$

$$T < 1. \tag{40}$$

When the external input signal *In* satisfies (13), we obtain the firing period of the nonlinking neuron as (40), which is always less than 1. However, the firing cycle of an ICM neuron can never be less than 1 inasmuch as the cycle should always be an integer greater than or equal to 1. The ICM neuron is invalid if the pulse cycle is less than 1; besides, we know that the ICM neuron is still invalid if $T = 1$ from Section IV.

Thus, we can infer that when the external input signal S satisfies

$$S < h\frac{(1-f)}{1-g} \tag{41}$$

the firing period of the nonlinking neuron satisfies

$$T > 1. \tag{42}$$

When (45) is satisfied, the neuron has the possibility of functioning properly. This conclusion is proven by our mathematical derivation in this section, which also validates (13).

For a linking neuron, the feedback input consists of the external input signal S and external coupled pulses. Compared with a nonlinking neuron, the feedback input tends to increase faster from the influence of external coupled pulses, which can be inferred by

$$F(n) = \left(S + \sum_{kl} W_{ijkl}Y(n-1)\right)\frac{1-f^n}{1-f}. \tag{43}$$

At the same time, the internal state of a linking neuron remains as $E(n) = gE(n-1)$, which is the same as a nonlinking neuron. As a result, the pulse of a linking neuron will be output in advance along with the future pulse. Thus, the pulse cycle of a linking neuron will be smaller than that of a nonlinking neuron.

In a linking neuron, it is very difficult to predict whether a neuron outputs a pulse using a mathematical analysis. Thus, we only discuss the firing characteristics of linking neurons based on the conclusions from nonlinking neurons. From those conclusions, we determine that the external input signal of a linking neuron must be less than that of a similar nonlinking neuron to keep the neuron working well.

Fig. 7. Commonly used images: (a) lena and (b) clock.

VII. EXPERIMENTS AND ANALYSIS

To verify the correctness of the mathematical analysis in this article, we used two common images as experimental samples, as shown in Fig. 7. After normalizing the image pixel values into the range "0–1," we added a constant to the normalized pixel values to move the minimum value close to the continuous firing condition; in addition, we removed coupling operations to observe the firing behavior of a single neuron, which can avoid the influence of the surrounding neurons. In the experiment, we used a completely black image to represent the output that is a single-value image, only 0 or 1, which means that all neurons output pulse or none output pulse. The completely black image means that the ICM network cannot extract any features of the source image. The other images indicate that some neurons output pulses while others do not, which means that the network can extract features from the source image.

For Fig. 7(a), we used the parameter values W= [1/8, 1/6, 1/8; 1/6, 0, 1/6; 1/8, 1/6, 1/8], $f = 0.85$, $g = 0.5$, and $h = 15$.

According to (13) and (20), the continuous firing condition for a nonlinking neuron can be calculated by (13) as 4.5; the continuous firing condition for a linking neuron can be calculated by (20) as 3.3333. Therefore, 4.5 is regarded as the continuous condition for keeping the neuron functioning well. In Fig. 8, the added constant is 3 to move each pixel value into the range "3–4," and all the pixel values are less than the continuous firing condition of 4.5. After the second iteration, all binary images are incomplete black images showing some output pulses but not others, which means that ICM neurons output the periodic pulse in their own cycle.

Fig. 9 represents the FSGs [see (4)] of the ICM network at the 50th, 70th, 90th, 150th, and 250th iterations. The differences between the highest and lowest pixel values of the FSGs are 10, 15, 20, 35, and 60, respectively. The changing difference shows that the pulse cycle of the neurons differs, and the binary images show that some neurons output pulses while others do not, which indicates that the network is functioning properly.

In Fig. 10, the added constant is 4.6 to shift pixels into the range of "4.6–5.6," with all pixel values larger than the continuous firing condition of 4.5, and this operation is similar to that of Fig. 8. As shown in Fig. 10, after the 20th iteration, all neurons fire continuously, and the experimental results are consistent with the theoretical conclusion.

Fig. 11 represents the FSGs of the network at the 50th, 70th, 90th, 150th, and 250th iterations. For different iterations, the differences between the highest and lowest values of the FSGs are 3, 3, 3, 3, and 3, respectively. In the previous

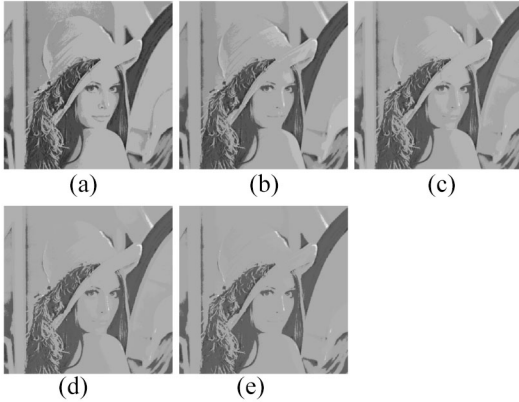Fig. 8. Binary images in different iterations (the constant is 3).

Fig. 9. FSGs at 50th, 70th, 90th, 150th, and 250th iterations with input signal *In*=3: (a) 50 iterations (25 maximum ignitions, 35 minimum ignitions); (b) 70 (35, 50); (c) 90 (45, 65); (d) 150 (75, 110); and (e) 250 (125, 185).
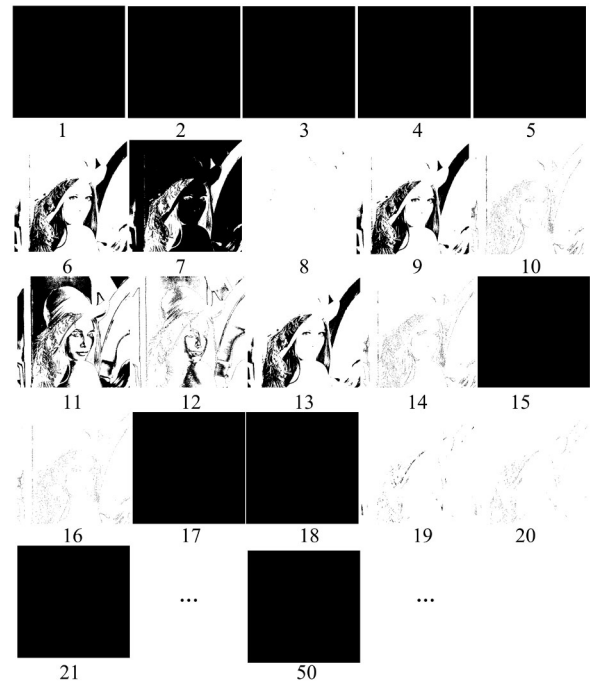

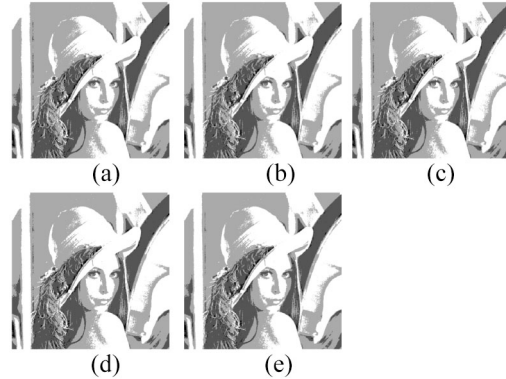Fig. 10. Binary images in different iterations (the constant is 4.6).

Fig. 11. FSGs at 50th, 70th, 90th, 150th, and 250th iterations with input signal In=4.6. (a) 50 iterations (44 maximum ignitions, 47 minimum ignitions). (b) 70 (64, 67). (c) 90 (84, 87). (d) 150 (144, 147). (e) 250 (244, 247).

20 iterations, some neurons output periodic pulses; however, the invariable difference shows that all neurons fire continuously at some iteration, indicating that the ICM network is invalid. The experiments show that our mathematical results are correct.

For Fig. 7(b), we use parameter values $f = 0.9$, $g = 0.8$, $h = 5$, and $W = [1/10, 1/6, 1/10; 1/6, 0, 1/6; 1/10, 1/6, 1/10]$, and the continuous firing condition can be calculated according to (13) and (20):

1) for a nonlinking neuron

$$S > h\frac{(1-f)}{(1-g)} = 5\frac{(1-0.9)}{(1-0.8)} = 5\frac{0.1}{0.2} = 2.5$$

2) for a linking ICM neuron

$$S > h\frac{(1-f)}{(1-g)} - \text{sum}(W) = 5\frac{(1-0.9)}{(1-0.8)} - \frac{16}{15} \approx 1.4333.$$

In Fig. 12, the added constant is 0.5 to move each pixel value into the range "1–1.5," and all the pixel values are less than the continuous firing condition of 2.5. After the first iteration, all binary images are incompletely black images showing some output pulses but not others, which means that ICM neurons output the periodic pulse in their own cycle.

Fig. 13 represents the FSGs of the ICM network at the 50th, 70th, 90th, 150th, and 250th iterations. The differences between the highest and lowest pixel values of the FSGs are 14, 21, 27, 46, and 79, respectively. The changing difference shows that the pulse cycle of the neurons differ.

In Fig. 14, the added constant is 2.6 to shift pixels into the range "2.6–3.6," with all pixel values larger than the continuous firing condition of 2.5. As shown in Fig. 14, after the 14th iteration all neurons fire continuously.

Fig. 15 represents the FSGs of the network at the 50th, 70th, 90th, 150th, and 250th iterations. For different iterations, the
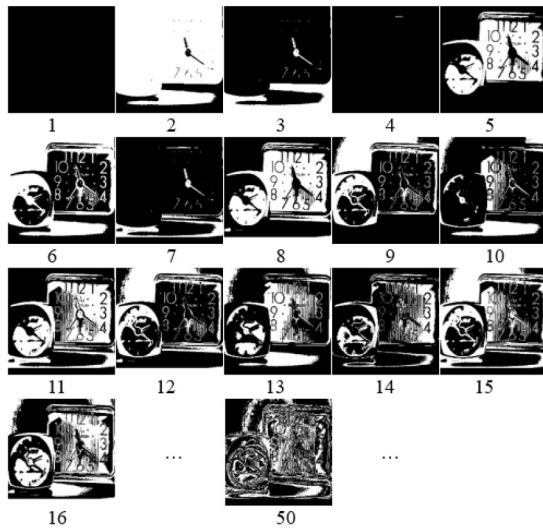
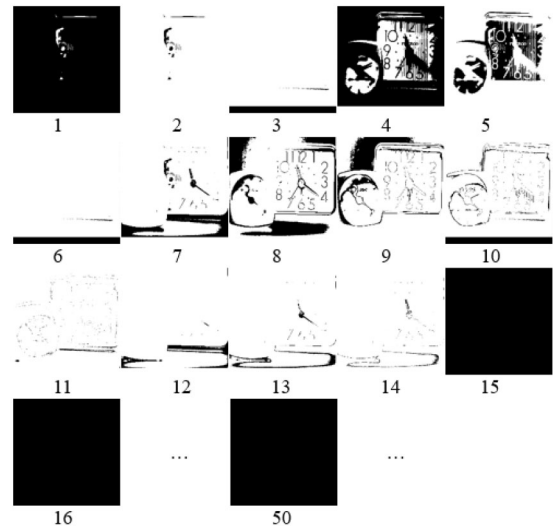Fig. 12. Binary images in different iterations (the constant is 0.5).

Fig. 14. Binary images in different iterations (the constant is 2.6).
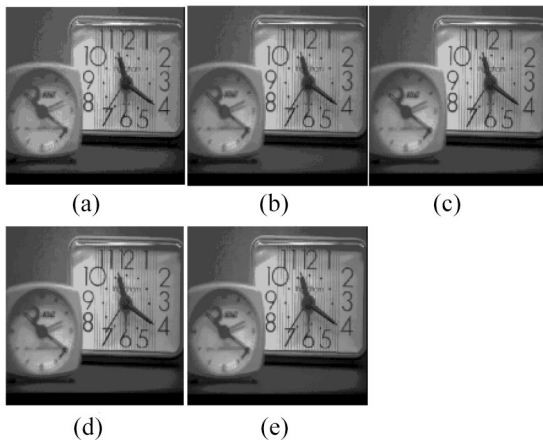

Fig. 13. FSGs at 50th, 70th, 90th, 150th, and 250th iterations. (a) 50 iterations (12 maximum ignitions, 26 ignitions). (b) 70 (17, 38). (c) 90 (22, 49). (d) 150 (37, 83). (e) 250 (62, 141).
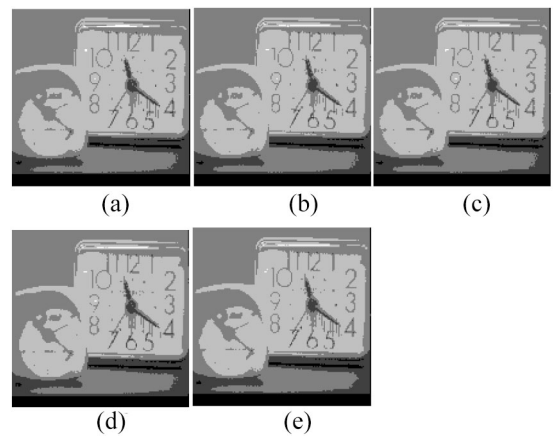

Fig. 15. FSGs at 50th, 70th, 90th, 150th, and 250th iterations. (a) 50 iterations (45 maximum ignitions, 49 minimum ignitions). (b) 70 (65, 69). (c) 90 (85, 89). (d) 150 (145, 149). (e) 250 (245, 249).

differences between the highest and lowest values of the FSGs are 4, 4, 4, 4, and 4, respectively. In the previous 15 iterations, some neurons output periodic pulses; however, the invariable difference shows that all neurons fire continuously at some iteration, indicating that the ICM network is invalid.

The experimental results in Figs. 12–15 are consistent with those in Figs. 8–11. From the experiments, we find that Figs. 9 and 13 present more detailed features than Figs. 11 and 15, which means that the neurons that satisfy the theoretical result will achieve better performance than the neurons that do not. Thus, our theoretical results are supported.

To further test the rationality of our work, we surveyed the previously published papers and organized the parameters into Table I, in which the condition of continuous firing of the non-linking and linking ICM neurons were calculated according to our theory, using (13) and (20). In [16], [28], and [29], the largest values of the normalized signals are "1," which are all less than the theoretical values of our work. The largest input pixel values in [33], [38], and [50] should be equal to (or less than) 256, which means the input signal is obviously less than

TABLE I
PARAMETERS OF ICM AND CONTINUOUS FIRING OF ICM NEURON
("–" REPRESENT UNKNOWN)

Ref.	Norm.	f	g	h	sum(W)	Eq. (13)	Eq. (20)
[28]	Yes	0.08	0.32	2	1	2.7059	1.7059
[16]	Yes	0.9	0.8	20	–	10	–
[29]	Yes	0.06	0.5	2	–	3.76	–
[33] [38]	No	0.9	0.7	1500	–	500	–
[50]	–	0.1	0.99	300	–	27000	–
[34]	–	0.9	0.8	20	–	10	–
[30] [39]	–	0.9	0.8	20	6.828	10	3.1720
[41]	–	0.9	0.8	250	6	125	119
[52]	–	0.1	0.9	5	–	45	–
[46] [47]	–	0	0.7408	20	1.3656	77.1605	75.7949

the theoretical values of our work. Besides, we can infer that the input signals in [30], [34], and [39] should be normalized according to [16]; although [41], [46], [47], [52] did not report if they had normalized operations, we can infer that our theoretical conditions were supported in some ways because our theoretical values were constants that should be greater than the largest input values. As a result, our theoretical results are supported by these previous works.

VIII. Conclusion

In this article, we focused on theoretical research concerning the firing mechanism of ICM neurons in order to provide better application foundations. We deduced the continuous firing condition of ICM neurons to determine the restrictions between the neuron parameters and the input signal, which is useful for formulating basic rules for ICM parameter selection. We then narrowed the scope of the ICM parameters according to our theoretical results. We also examined the neuron pulse cycle to understand the neural firing mechanism according to its firing condition. The continuous firing condition and the pulse cycle of neurons are useful to prove the reasonable values for each other. The mathematical analysis helps in understanding the neural firing mechanism and guides parameter selection to create a network that functions well. In addition, this research provides an available way to study other versions of the PCNN because of the similar characteristics between the ICM and PCNN. The experimental results confirm the validity of our mathematical results and conclusions. In the future, we plan to focus on parameter optimization in view of the firing mechanism and the specific application of our theory.

References

[1] H. Qu, Z. Yi, and S. X. Yang, "Efficient shortest-path-tree computation in network routing based on pulse-coupled neural networks," *IEEE Trans. Cybern.*, vol. 43, no. 3, pp. 995–1010, Jun. 2013.

[2] C. Panigrahy, A. Seal, and N. Mahato, "MRI and SPECT image fusion using a weighted parameter adaptive dual channel PCNN," *IEEE Signal Process. Lett.*, vol. 27, pp. 690–694, 2020.

[3] H. Sang and J. Zhao, "Sampled-data-based H∞ synchronization of switched coupled neural networks," *IEEE Trans. Cybern.*, early access, Apr. 22, 2019, doi: 10.1109/TCYB.2019.2908187.

[4] S. Guo, Z. Yu, F. Deng, X. Hu, and F. Chen, "Hierarchical Bayesian inference and learning in spiking neural networks," *IEEE Trans. Cybern.*, vol. 49, no. 1, pp. 133–145, Jan. 2019.

[5] S. Valadez-Godínez, H. Sossa, and R. Santiago-Montero, "On the accuracy and computational cost of spiking neuron implementation," *Neural Netw.*, vol. 122, pp. 196–217, Feb. 2020.

[6] H. Wang, J. Peng, and S. Yue, "A directionally selective small target motion detecting visual neural network in cluttered backgrounds," *IEEE Trans. Cybern.*, vol. 50, no. 4, pp. 1541–1555, Apr. 2020.

[7] R. Lan *et al.*, "Cascading and enhanced residual networks for accurate single-image super-resolution," *IEEE Trans. Cybern.*, early access, Feb. 21, 2020. [Online]. Available: https://doi.org/10.1109/TCYB.2019.2952710

[8] R. Eckhorn, H. Reitboeck, M. Arndt, and P. Dicke, "Feature linking via synchronization among distributed assemblies: Simulations of results from cat visual cortex," *Neural Comput.*, vol. 2, no. 3, pp. 293–307, Sep. 1990.

[9] A. J. M. Kinser, "Simplified pulse-coupled neural network," in *Proc. SPIE Appl. Sci. Artif. Neural Netw.*, vol. 2760, 1996, pp. 563–567.

[10] X. Jin *et al.*, "A novel DNA sequence similarity calculation based on simplified pulse-coupled neural network and Huffman coding," *Physica A, Stat. Mech. Appl.*, vol. 461, pp. 325–338, Nov. 2016.

[11] H. Zhuang, K.-S. Low, and W.-Y. Yau, "Multichannel pulse-coupled-neural-network-based color image segmentation for object detection," *IEEE Trans. Ind. Electron.*, vol. 59, no. 8, pp. 3299–3308, Aug. 2012.

[12] J. Xin, C. Gao, H. Jingyu, J. Qian, Z. Dongming, and Y. Shaowen, "Multimodal sensor medical image fusion based on nonsubsampled shearlet transform and S-PCNNs in HSV space," *Signal Process.*, vol. 153, pp. 379–395, Dec. 2018.

[13] P. Duan, X. Kang, S. Li, and P. Ghamisi, "Multichannel pulse-coupled neural network-based hyperspectral image visualization," *IEEE Trans. Geosci. Remote Sens.*, vol. 58, no. 4, pp. 2444–2456, Apr. 2020.

[14] Q. Kang, B. Huang, and M. Zhou, "Dynamic behavior of artificial Hodgkin–Huxley neuron model subject to additive noise," *IEEE Trans. Cybern.*, vol. 46, no. 9, pp. 2083–2093, Sep. 2016.

[15] U. Ekblad and J. Kinser, "Theoretical foundation of the intersecting cortical model and its use for change detection of aircraft, cars, and nuclear explosion tests," *Signal Process.*, vol. 84, no. 7, pp. 1131–1146, 2004.

[16] U. Ekblad, J. Kinser, J. Atmer, and N. Zetterlund, "The intersecting cortical model in image processing," *Nucl. Instrum. Methods Phys. Res. A, Accelerators Spectrometers Detectors Assoc. Equip.*, vol. 525, nos. 1–2, pp. 392–396, 2004.

[17] K. Zhan, J. Shi, H. Wang, Y. Xie, and Q. Li, "Computational mechanisms of pulse-coupled neural networks: A comprehensive review," *Archives Comput. Meth. Eng.*, vol. 24, no. 3, pp. 573–588, 2017.

[18] A. Lakshmi and S. Ravi, "Automated segmentation algorithm for cervical cell images by employing cuckoo search based ICM," *J. Ambient Intell. Human Comput.*, to be published. [Online]. Available: https://doi.org/10.1007/s12652-017-0640-z

[19] Z. Wang, Y. Ma, F. Cheng, and L. Yang, "Review of pulse-coupled neural networks," *Image Vis. Comput.*, vol. 28, no. 1, pp. 5–13, 2010.

[20] C. Wang, L. He, S. Ma, and S. Gao, "Superpixel-based saliency guided intersecting cortical model for unsupervised object segmentation," in *Proc. 10th Int. Conf. Image Graph.*, 2019, pp. 3–17.

[21] H. Peng, J. Wang, M. J. Perez-Jiménez, and A. Riscos-Núñez, "Dynamic threshold neural P systems," *Knowl. Based Syst.*, vol. 163, pp. 875–884, Jan. 2019.

[22] Y. Chen, Y. Ma, D. H. Kim, and S. Park, "Region-based object recognition by color segmentation using a simplified PCNN," *IEEE Trans. Neural Netw. Learn. Syst.*, vol. 26, no. 8, pp. 1682–1697, Aug. 2015.

[23] M. Subashini and S. Sahoo, "Pulse coupled neural networks and its applications," *Expert Syst. Appl.*, vol. 41, no. 8, pp. 3965–3974, 2014.

[24] M. Harris, A. Van, B. Malik, J. M. Jabbour, and K. C. Maitland, "A pulse coupled neural network segmentation algorithm for reflectance confocal images of epithelial tissue," *PLoS ONE*, vol. 10, no. 3, 2015, Art. no. e0122368.

[25] Y. Chen, S. Park, Y. Ma, and R. Ala, "A new automatic parameter setting method of a simplified PCNN for image segmentation," *IEEE Trans. Neural Netw.*, vol. 22, no. 6, pp. 880–892, Jun. 2011.

[26] R. Broussard, S. Rogers, M. Oxley, and G. L. Tarr, "Physiologically motivated image fusion for object detection using a pulse coupled neural network," *IEEE Trans. Neural Netw.*, vol. 10, no. 3, pp. 554–563, May 1999.

[27] U. Ekblad, "Earth satellites and air and ground-based activities," Ph.D. dissertation, Dept. Physics, Roy. Inst. Technol., Stockholm, Sweden, 2004.

[28] G. Xu, Z. Zhang, and Y. Ma, "A novel method for iris feature extraction based on intersecting cortical model network," *J. Appl. Math. Comput.*, vol. 26, no. 1, pp. 341–352, 2008.

[29] F. Mokhayeri and M. Akbarzadeh-T, "A novel facial feature extraction method based on ICM network for affective recognition," in *Proc. Int. Joint Conf. Neural Netw. (IJCNN)*, San Jose, CA, USA, 2011, pp. 1988–1993.

[30] Y. Ma, L. Liu, K. Zhan, and Y. Wu, "Pulse-coupled neural networks and one-class support vector machines for geometry invariant texture retrieval," *Image Vis. Comput.*, vol. 28, no. 11, pp. 1524–1529, 2010.

[31] R. Yu, B. Zhu, K. Zhang, and M. Lv, "An image matching recognition approach based on ICM icon," in *Proc. IEEE 5th Int. Conf. Fuzzy Syst. Knowl. Discov.*, Shandong, China, 2008, pp. 20–23.

[32] Z. Wang *et al.*, "Plant recognition based on intersecting cortical model," in *Proc. Int. Joint Conf. Neural Netw. (IJCNN)*, Beijing, China, Jul. 2014, pp. 975–980.

[33] Q. Gao and L. Zhang, "An unstructured lane detection algorithm based on intersecting cortical model," *Acta Electronica Sinica*, vol. 39, no. 10, pp. 2366–2371, 2011.

[34] A, Mahgoub, A. Ebeid, H. Abdel-Baky, and E. A. El-Badawy, "An intersecting cortical model based framework for human face recognition," *J. Syst. Cybern. Informat.*, vol. 6, no. 2, pp. 213–215, 2008.

[35] P. Gao, L. Li, and X. Chen, "Dynamic linear threshold attenuation linking synaptic computing network for image enhancement," *J. Electron. Imag.*, vol. 28, no. 5, pp. 1–12, 2019.

[36] Z. Zhen, "An image segmentation algorithm based on combination of slope width reduction and cross cortical model," *Int. J. Comput. Appl. Technol.*, vol. 61, nos. 1–2, pp. 75–80, 2019.

[37] W. Tan and M. Ashidi, "Automated sperm head detection using intersecting cortical model optimised by particle swarm optimization," *PLoS ONE*, vol. 11, no. 9, 2016, Art. no. e0162985.

[38] H. Wang, M. Li, Y. Li, and K. Zhang, "An image fusion method based on wavelet transform and ICM," in *Proc. SPIE Int. Conf. Space Inf. Technol.*, vol. 7651, 2010, Art. no. 855426.

[39] C. Kavitha, C. Chellamuthu, and R. Rajesh, "Multimodal medical image fusion using discrete Ripplet transform and intersecting cortical model," *Proc. Eng.*, vol. 38, no. 1, pp. 1409–1414, 2012.

[40] W. Kong, "Multi-sensor image fusion based on NSST domain I^{2}CM," *Electron. Lett.*, vol. 49, no. 13, pp. 802–803, Jun. 2013.

[41] X. Jin, D. Zhou, S. Yao, R. Nie, C. Yu, and T. Ding, "Remote sensing image fusion method in CIELab color space using nonsubsampled shearlet transform and pulse coupled neural networks," *J. Appl. Remote Sens.*, vol. 10, no. 2, 2016, Art. no. 025023.

[42] N. Wang, Y. Ma, and K. Z. Han, "Spiking cortical model for multifocus image fusion," *Neurocomputing*, vol. 130, no. 3, pp. 44–51, 2012.

[43] L. Yang, "Multi-focus image fusion method based on NSST and IICM," in *Advances in Internetworking, Data and Web Technologies (EIDWT)* (Lecture Notes on Data Engineering and Communications Technologies), vol. 6. Cham, Switzerland: Springer, 2017.

[44] Q. Wang, Y. Lei, C. Ren, and M. Li, "Spiking cortical model: A new member in the third generation of artificial neural network," in *Proc. 3rd Int. Conf. Electron. Inf. Technol. Comput. Eng. (EITCE)*, 2019, pp. 1883–1887.

[45] B. Li, H. Peng, J. Wang, and X. Huang, "Multi-focus image fusion based on dynamic threshold neural P systems and surfacelet transform," *Knowl. Based Syst.*, vol. 196, May 2020, Art. no. 105794.

[46] J. Yuan, H. Zhang, and Y. Ma, "Effectual switching filter for removing impulse noise using a SCM detector," *Opt. Eng.*, vol. 51, no. 3, 2012, Art. no. 037003.

[47] Y. Ma, J. Yuan, and H. Zhang, "Self-adaptive method using SCM for noise removal in color images," *J. Univ. Electron. Sci. Technol. China*, vol. 41, no. 5, pp. 754–758, 2012.

[48] X. Zhang, Z. Zheng, I. Asanuma, and Y. Xu, "A new kind of hybrid filter based on the intersecting cortical model and the improved extremum-and-median filter," *Artif. Life Robot.*, vol. 19, no. 2, pp. 115–119, 2014.

[49] S. Nisha and K. Mohideen, "Noise removal in medical images using pulse coupled neural networks," *J. Med. Imag. Health Informa.*, vol. 7, no. 1, pp. 101–105, 2017.

[50] S. Gao, C. Li, and D. Bi, "Image enhancement algorithm based on NF-ICM," *Chin. Opt. Lett.*, vol. 8, no. 5, pp. 474–477, 2010.

[51] A. Baddeley and M. Lieshout, "ICM for object recognition," in *Computational Statistics*. Heidelberg, Germany: Physica-Verlag, 1992, pp. 271–286.

[52] C. Li, C. Wang, M. Ju, S. Gao, and D. Bi, "Visualization of high dynamic range image based on intersecting cortical model," *J. Comput.-Aided Design Comput. Graph.*, vol. 23, no. 8, pp. 1420–1426, 2011.

[53] C. Li, P. Wang, and Y. Bi, "Realistic image rendition based on intersecting cortical model," *J. Univ. Electron. Sci. Technol. China*, vol. 47, no. 2, pp. 272–278, 2018.

[54] W. C. Tan and N. A. M. Isa, "Single sperm tracking using intersect cortical model-mean shift method," in *Proc. Int. Conf. Signals Syst. (ICSigSys)*, Sanur, Indonesia, 2017, pp. 221–226.

[55] X. Xu, G. Wang, S. Ding, Y. Cheng, and X. Wang, "Pulse-coupled neural networks and parameter optimization methods," *Neural Comput. Appl.*, vol. 28, no. S1, pp. 671–681, 2017.

[56] X. Jin *et al.*, "Multi-focus image fusion method using S-PCNN optimized by particle swarm optimization," *Soft Comput.*, vol. 22, no. 19, pp. 6395–6407, 2018.

[57] R. Nie, J. Cao, D. Zhou, and W. Qian, "Analysis of pulse period for passive neuron in pulse coupled neural network," *Math. Comput. Simul.*, vol. 155, pp. 277–289, Jan. 2019,

[58] R. Nie, "Research on theory analysis and application for critical characteristic of pulse coupled neural network," Ph.D. dissertation, Dept. School Inf., Yunnan Univ., Kunming, China, 2014.

[59] M. Yin, X. Liu, Y. Liu, and X. Chen, "Medical image fusion with parameter-adaptive pulse coupled neural network in nonsubsampled shearlet transform domain," *IEEE Trans. Instrum. Meas.*, vol. 68, no. 1, pp. 49–64, Jan. 2019.
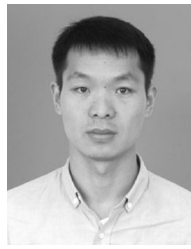
Xin Jin (Member, IEEE) received the B.S. degree in electronics and information engineering from Henan Normal University, Xinxiang, China, in 2013, and the Ph.D. degree in communication and information systems from Yunnan University, Kunming, China, in 2018.

He is a Postdoctoral Researcher with the School of Software, Yunnan University. His current research interests include pulse coupled neural-network theory and its applications, image processing, optimization algorithms, and bioinformatics.

Dongming Zhou received the B.S. and M.S. degrees in automatic control engineering from the Huazhong University of Science and Technology, Wuhan, China, in 1985 and 1988, respectively, and the Ph.D. degree in electronic circuits and systems from Fudan University, Shanghai, China, in 2004.

He is a Professor with the School of Information, Yunnan University, Kunming, China. His current research interests include neural-network theory and applications, artificial-intelligence control theory, and image processing.

Qian Jiang received the B.S. degree in thermal energy and power engineering and the M.S. degree in power engineering and engineering thermophysics from Central South University, Changsha, China, in 2012 and 2015, respectively.

She is a Postdoctoral Researcher with the School of Software, Yunnan University, Kunming, China. Her research interests include machine learning, bioinformatics, and image processing.

Xing Chu (Member, IEEE) received the B.E. degree from the Kunming University of Science and Technology, Kunming, China, in 2011, the M.E. degree from Hunan University, Changsha, China, in 2014, and the Ph.D. degree in control theory and engineering from the École Centrale de Lille, Villeneuve-d'Ascq, France, in 2017.

He is a Lecturer with the School of Software, Yunnan University, Kunming. His research interests lie in distributed cooperative control of multiagent/robot systems and intelligent automobiles.

Shaowen Yao (Member, IEEE) received the B.S. and M.S. degrees in telecommunication engineering from Yunnan University, Kunming, China, in 1988 and 1991, respectively, and the Ph.D. degree in computer application technology from the University of Electronic Science and Technology of China, Chengdu, China, in 2002.

He is a Professor with the School of Software, Yunnan University. His current research interests include neural-network theory and applications, cloud computing, and big data computing.

Wei Zhou (Member, IEEE) received the Ph.D. degree from the University of Chinese Academy of Science, Beijing, China, in 2008.

He is a Professor with the School of Software, Yunnan University, Kunming, China, where he is currently a Full Professor. His current research interests include distributed data intensive computing and bioinformatics.

Keqin Li (Fellow, IEEE) received the Ph.D. degree in computer science from the University of Houston, Houston, TX, USA, in 1990. He is a SUNY Distinguished Professor of Computer Science with the State University of New York, New Paltz, NY, USA. He has published over 760 journal articles, book chapters, and refereed conference papers. His current research interests include cloud computing, fog computing and mobile edge computing, energy-efficient computing and communication, embedded systems and cyber-physical systems, heterogeneous computing systems, big data computing, high-performance computing, CPU–GPU hybrid and cooperative computing, computer architectures and systems, computer networking, machine learning, and intelligent and soft computing.

Dr. Li has received several best paper awards. He has served on the editorial boards of the IEEE TRANSACTIONS ON PARALLEL AND DISTRIBUTED SYSTEMS, the IEEE TRANSACTIONS ON COMPUTERS, the IEEE TRANSACTIONS ON CLOUD COMPUTING, the IEEE TRANSACTIONS ON SERVICES COMPUTING, and the IEEE TRANSACTIONS ON SUSTAINABLE COMPUTING.